Molecular Therapy
Nucleic Acids
Original Article

miR-146a inhibits mitochondrial dysfunction and myocardial infarction by targeting cyclophilin D

Qiang Su,[1] Yuli Xu,[1] Ruping Cai,[1] Rixin Dai,[1] Xiheng Yang,[1] Yang Liu,[2] and Binghui Kong[3]

[1]Department of Cardiology, The Affiliated Hospital of Guilin Medical University, Guilin 541001, Guangxi, China; [2]Department of Cardiology, The Second People's Hospital of Nanning City, The Third Affiliated Hospital of Guangxi Medical University, Nanning 530031, Guangxi, China; [3]Department of Cardiology, The First Affiliated Hospital of Guangxi Medical University, Nanning 530021, Guangxi, China

Increasing evidence suggests that mitochondrial microRNAs (miRNAs) are implicated in the pathogenesis of cardiovascular diseases; however, their roles in ischemic heart disease remain unclear. Herein, we demonstrate that miR-146a is enriched in the mitochondrial fraction of cardiomyocytes, and its level significantly decreases after ischemic reperfusion (I/R) challenge. Cardiomyocyte-specific knockout of miR-146a aggravated myocardial infarction, apoptosis, and cardiac dysfunction induced by the I/R injury. Overexpression of miR-146a suppressed anoxia/reoxygenation-induced cardiomyocyte apoptosis by inhibiting the mitochondria-dependent apoptotic pathway and increasing the Bcl-2/Bax ratio. miR-146a overexpression also blocked mitochondrial permeability transition pore opening and attenuated the loss of mitochondrial membrane potential and cytochrome *c* leakage; meanwhile, miR-146a knockdown elicited the opposite effects. Additionally, miR-146a overexpression decreased cyclophilin D protein, not mRNA, expression. The luciferase reporter assay revealed that miR-146a binds to the coding sequence of the cyclophilin D gene. Restoration of cyclophilin D reversed the inhibitory action of miR-146a on cardiomyocyte apoptosis. Furthermore, cardiomyocyte-specific cyclophilin D deletion completely abolished the exacerbation of myocardial infarction and apoptosis observed in miR-146a cardiomyocyte-deficient mice. Collectively, these findings demonstrate that nuclear miR-146a translocates into the mitochondria and regulates mitochondrial function and cardiomyocyte apoptosis. Our study unveils a novel role for miR-146a in ischemic heart disease.

INTRODUCTION

Myocardial infarction, which is characterized by prolonged ischemia of the coronary arteries, remains the leading cardiovascular cause of death worldwide.[1] Blood flow restoration to the ischemic myocardium is currently the most timely and effective strategy to improve the outcome of patients with acute myocardial infarction.[2] However, such restoration often leads to ischemic reperfusion (I/R) injury.[3] Apoptosis of the terminally differentiated cardiomyocytes has been documented as an important pathogenic factor involved in cardiac I/R injury.[4] Evidence has accumulated showing that the suppression of cardiomyocyte apoptosis is beneficial for decreasing infarction size and improving myocardial contractile dysfunction after reperfusion, suggesting that this manipulation may be a useful approach for protection against I/R injury.[4,5] Nevertheless, the fundamental mechanisms underlying cardiomyocyte apoptosis are poorly understood.

A large body of evidence has indicated that mitochondrial dysfunction is associated with the development of many diseases, including cardiovascular disorders.[4,6,7] Cardiomyocytes contain many mitochondria; hence, mitochondria-dependent apoptosis affects cardiomyocyte survival.[4,8] The mechanisms by which mitochondria-dependent apoptosis is regulated include the cyclophilin D-mitochondrial permeability transition pore (mPTP) opening, subsequent disruption of mitochondrial membrane potential (MMP), cytochrome *c* release, and caspase activation, which collectively lead to mitochondrial dysfunction.[9] Therefore, the maintenance of mitochondrial structure and homeostasis is a promising strategy for the amelioration of cardiomyocyte apoptosis and cardiac injury.[7,8,10]

MicroRNAs (miRNAs) are a class of non-coding 12- to 23-nucleotide RNAs that regulate gene expression at the posttranscriptional level.[4–6] miRNAs have been found to play roles in cardiac dysfunctions, such as heart failure, cardiac hypertrophy, and ischemic injury.[4,5,7,10] miR-146 was initially identified as a critical regulator of hematopoiesis, inflammation, and immunity.[11] However, more recently it was shown to also be associated with the development of cardiovascular diseases, including doxorubicin cardiotoxicity, diabetic cardiomyopathy, and atherosclerosis.[12–14] Interestingly, emerging evidence suggests the presence and regulatory roles of miRNAs in the mitochondria.[4,7,10] In the present study, we for the first time demonstrate that miR-146a localizes to the mitochondria, where its level dramatically

Received 30 July 2020; accepted 28 January 2021;
https://doi.org/10.1016/j.omtn.2021.01.034.

Correspondence: Qiang Su, Department of Cardiology, The Affiliated Hospital of the Guilin Medical University, 15#, Lequn Road, Guilin 541001, Guangxi, China.
E-mail: suqiang1983@foxmail.com

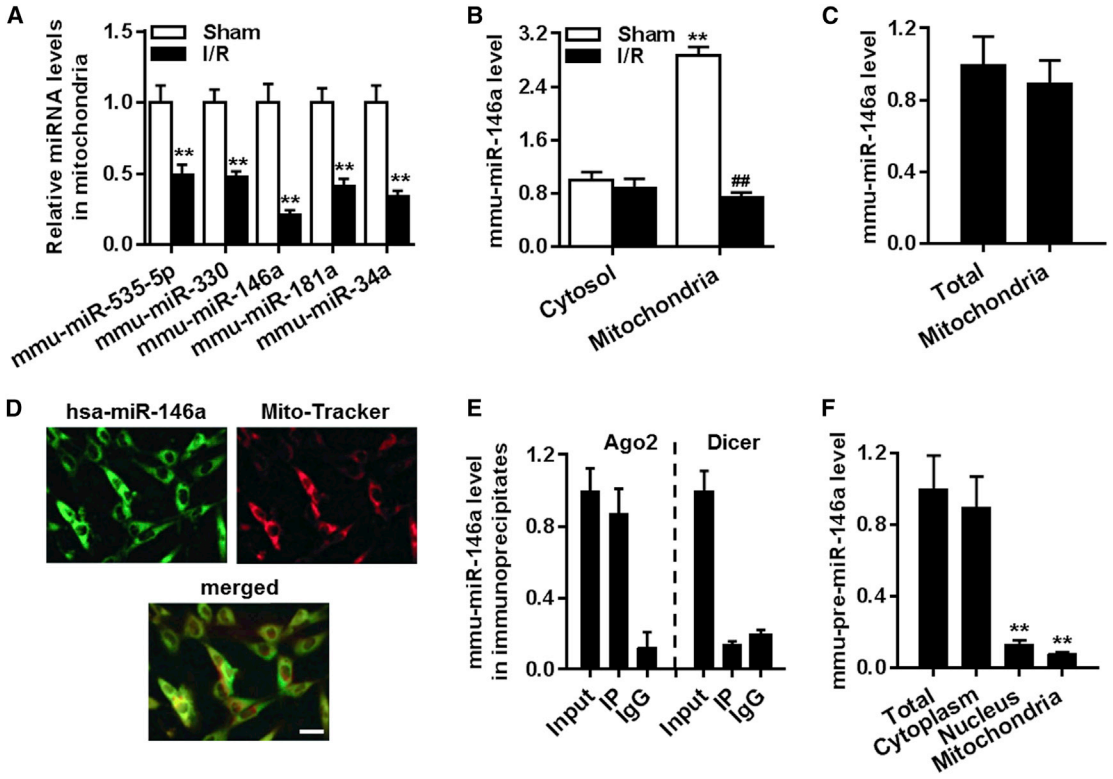

Figure 1. Decreased level of miR-146a in the mitochondria after cardiac ischemia/reperfusion (I/R) injury

(A) miRNA-enriched RNA was isolated from the mitochondrial fraction of mouse myocardia after sham surgery or I/R injury. Downregulation of miRNAs observed in miRNA microarray experiments was verified by qRT-PCR. **$p < 0.01$ versus sham, n = 6. (B) miR-146a levels in the cytosolic and mitochondrial fractions of the myocardium in response to I/R challenge and following sham surgery. **$p < 0.01$ versus cytosol sham; $^{\#\#}p < 0.01$ versus mitochondria sham, n = 6. (C) miR-146a levels in the whole heart and mitochondrial fractions determined by qRT-PCR (n = 4). (D) Fluorescence *in situ* hybridization demonstrates miR-146a localization in mitochondria. Representative images of one of the four similar experiments are presented. (E) qRT-PCR analysis of miR-146a level in the Ago2 or dicer immunoprecipitate from the mitochondrial fraction (n = 4). (F) pre-miR-146a levels in the total heart tissue, nuclear, and mitochondrial fractions. **$p < 0.01$ versus total heart, n = 6.

changes after an I/R episode. Although the influence of miR-146a, mediated by a conventional miRNA-regulated pathway, on I/R injury had been proposed previously, our findings reveal a novel role and mechanism of action for mitochondrial miR-146 in cardiac I/R injury. Herein, we demonstrate that mitochondrial miR-146a is a key regulator of mitochondrial dysfunction, cardiomyocyte apoptosis, and heart ischemic disease.

RESULTS

Mitochondrial miR-146a is downregulated in the myocardium under I/R conditions

Microarray analysis of the heart mitochondrial fraction identified 15 miRNAs that were differentially expressed in the tissues of sham-operated control mice and mice that underwent I/R. Among the 15 dysregulated miRNAs, miR-535-5p, miR-330, miR-146a, miR-181a, and miR-34a were significantly downregulated. The difference of miR-146a levels was the most pronounced compared to the changes in other mitochondrial miRNAs (Table S3). This was further confirmed by qRT-PCR, in which mitochondrial 12S rRNA was used as an internal control (Figure 1A). Thus, we decided to focus on the role of miR-146a, which is conserved between mice and humans (Figure S1A), in cardiac I/R injury. We found that miR-146a was enriched primarily in the mitochondrial fraction compared to its level in the cytosolic fraction. I/R challenge significantly reduced miR-146a level in the mitochondria but not in the cytosol (Figure 1B). In line with the *in vivo* results, miR-146a level in cardiomyocytes was decreased upon anoxia/reoxygenation (A/R) treatment in a time-dependent manner (Figure S1B). We also observed that A/R challenge led to a significant reduction in intracellular ATP levels (Figure S1C), which is a hallmark of mitochondrial dysfunction. Interestingly, the miR-146a level was positively correlated with ATP level, with a correlation coefficient of 0.8581 (Figure S1D), suggesting that mitochondrial miR-146a may play a role in mitochondrial dysfunction during cardiac I/R injury. Moreover, qRT-PCR results revealed that the abundance of miR-146a in the mitochondrial fraction was similar to that in the whole heart, suggesting that miR-146a is predominantly localized in the mitochondria (Figure 1C). Fluorescence *in situ* hybridization confirmed that miR-146a was present in the mitochondria of cardiomyocytes (Figure 1D).

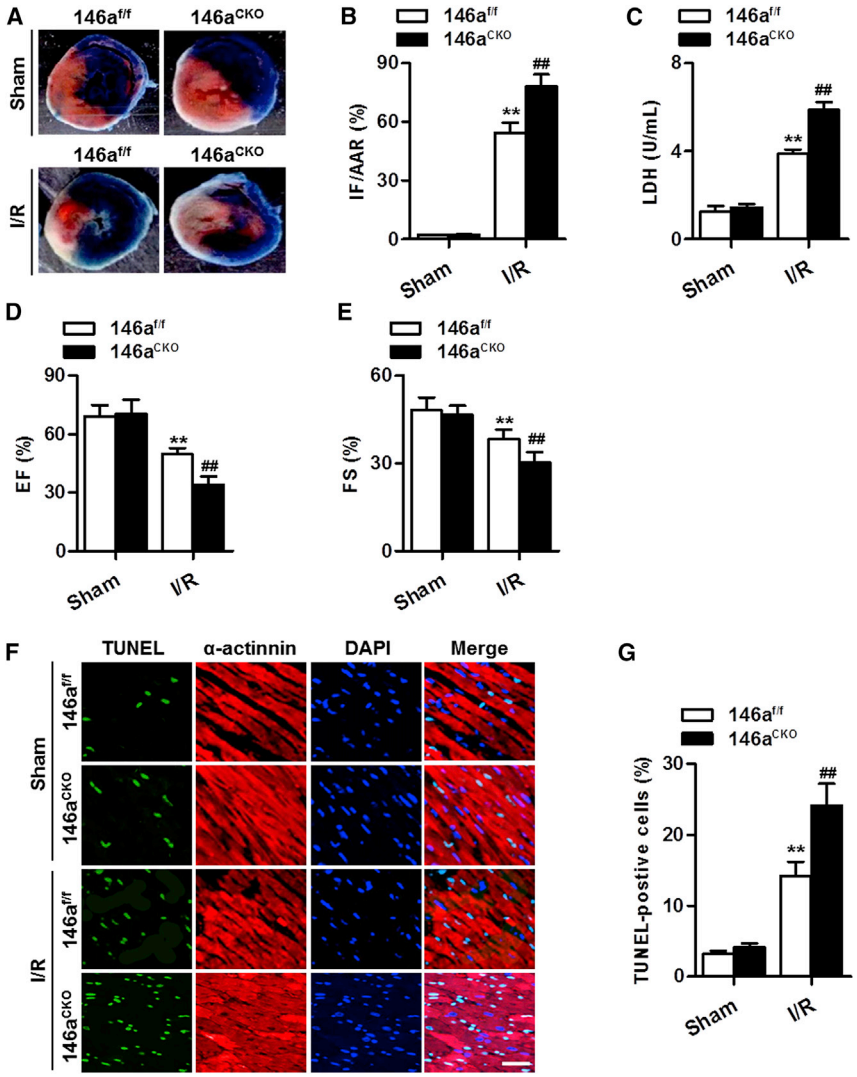

Figure 2. Deficiency of miR-146a in cardiomyocytes exacerbates I/R injury

(A) Cardiomyocyte-specific miR-146a knockout mice ($146a^{CKO}$) and their control littermates ($146a^{f/f}$) received I/R (30 min ischemia and 4 h reperfusion) or sham treatment. Representative images of myocardial tissue sections are shown. (B) Myocardial infarct size expressed as the ratio of infarcted area (IF) to the area at risk (AAR) (IF/AAR). $^{**}p < 0.01$ versus sham $146a^{f/f}$; $^{\#\#}p < 0.01$ versus sham $146a^{CKO}$, n = 6 per group. (C) Lactate dehydrogenase (LDH) level in serum was measured by a commercial kit. $^{**}p < 0.01$ versus sham $146a^{f/f}$; $^{\#\#}p < 0.01$ versus sham $146a^{CKO}$, n = 12–16 per group. (D and E) Echocardiographic analysis of left ventricular ejection fraction (EF) (D) and left ventricular fractional shortening (FS) (E) at the end of 24 h reperfusion. $^{**}p < 0.01$ versus sham $146a^{f/f}$; $^{\#\#}p < 0.01$ versus sham $146a^{CKO}$, n = 8–10 per group. (F) Representative images of TUNEL and α-actinin staining of myocardial tissue sections after 30 min myocardial ischemia followed by 4 h reperfusion. Green TUNEL staining represents apoptotic cells, cardiomyocytes are labeled with an anti-α-actinin antibody showing red color, and the nuclei are stained blue by 4′,6-diamidino-2-phenylindole (DAPI). (G) Quantification of apoptotic cardiomyocytes in each group. $^{**}p < 0.01$ versus sham $146a^{f/f}$; $^{\#\#}p < 0.01$ versus sham $146a^{CKO}$, n = 7 per group.

Ago2 has been shown to localize in the mitochondria and play an important role in the translocation of miRNAs into the mitochondria.[4,7] Additionally, dicer, which generates miRNA maturation from primary miRNA, is present exclusively in the cytoplasm, not in mitochondria.[7] As expected, we observed that Ago2 was expressed both in cytosolic and mitochondrial fractions of cardiomyocytes, while dicer was largely absent from mitochondria (Figure S2). Moreover, the RNA-binding protein immunoprecipitation (RIP) experiment showed that miR-146a in the mitochondrial fraction was co-immunoprecipitated with Ago2, not dicer (Figure 1E), confirming mitochondrial localization of miR-146a. To investigate miR-146a biogenesis, we examined the presence of pre-miR-146a in the whole heart, as well as in the nuclear, cytosolic, and mitochondrial fractions. Results show that minimal levels of pre-miR-146a were observed in the nuclear and mitochondrial fractions compared with that in the total heart homogenate (Figure 1F). This indicates that miR-146a biosynthesis occurs in a conventional manner, with miR-146a translocating into the mitochondria following maturation in the cytosol.

Cardiomyocyte-specific knockout of miR-146a exacerbates cardiac I/R injury

To investigate the association between the downregulation of miR-146a and I/R-induced myocardial injury, we performed I/R surgery in miR-146a cardiomyocyte-specific knockout mice (Figure S3). As shown in Figure 2A, no infarct was observed in the myocardium of $miR\text{-}146a^{f/f}$ mice and $miR\text{-}146a^{CKO}$ mice under sham conditions. Mice that underwent I/R revealed an apparent infarct, which was significantly aggravated by cardiomyocyte-specific deficiency of miR-146a (Figure 2B). The release of lactate dehydrogenase (LDH), a marker for cardiac injury, was expectedly increased after I/R injury. Knockout of miR-146a further increased the level of LDH (Figure 2C). Echocardiography examination showed that the impairment of cardiac function was exacerbated in $miR\text{-}146a^{CKO}$ mice, as evidenced by lower values of ejection fraction (EF) and fractional shortening (FS) (Figures 2D and 2E). Cardiomyocyte apoptosis is an important contributor to myocardial dysfunction and failure. Transferase dUTP nick end labeling (TUNEL) staining revealed no significant difference in the number of cardiomyocytes undergoing apoptosis in the myocardium between $miR\text{-}146a^{f/f}$ and $miR\text{-}146a^{CKO}$ mice under sham conditions. I/R stimulation markedly increased the number of apoptotic cells, and this increase was further enhanced by cardiomyocyte-specific knockout of miR-146a (Figures 2F and 2G).

miR-146a upregulation ameliorates A/R-induced cardiomyocyte apoptosis *in vitro*

We next examined whether the regulatory role of miR-146a in cardiomyocyte apoptosis was also evident *in vitro*, under A/R conditions. The annexin V-fluorescein isothiocyanate (FITC)/propidium iodide (PI) assay showed that the ratio of apoptotic cells did not change after overexpression or knockdown of miR-146a, as compared with that in the relevant negative control experiment. A/R treatment markedly enhanced the fraction of apoptotic cardiomyocytes, which was inhibited by miR-146a upregulation yet further augmented by miR-146a knockdown (Figures 3A and 3B). In addition, TUNEL staining also demonstrated that overexpression of miR-146a markedly attenuated apoptosis of cardiomyocytes induced by A/R, whereas downregulation of miR-146a was associated with enhanced cell apoptosis (Figures 3C and 3D). Given the alterations of miR-146a in the mitochondria, we explored whether miR-146a affects the mitochondria-dependent apoptotic pathway and cardiomyocyte survival. The anti-apoptotic Bcl-2 protein family and the pro-apoptotic Bax protein from the same family are essential for the initiation of mitochondrial apoptosis. Lower expression of Bcl-2 and higher expression of Bax were found in A/R-treated cardiomyocytes compared with the respective levels in untreated cells. The Bcl-2/Bax ratio, which determines the fate of cell survival, was significantly decreased by A/R. miR-146a upregulation reversed A/R-induced decrease in the Bcl-2/Bax ratio by increasing Bcl-2 expression and attenuating Bax expression. However, miR-146a downregulation further augmented the effects of A/R on Bcl-2 and Bax expression levels and the Bcl-2/Bax ratio (Figures 3E and 3F).

miR-146a attenuates mitochondrial dysfunction under A/R conditions

The loss of MMP leading to mitochondrial dysfunction is considered as the predominant consequence of the imbalance between Bcl-2 and Bax expression levels. We thus determined the effects of miR-146a on MMP in cardiomyocytes by using 5,5′,6,6′-tetrachloro-1,1′,3,3′-tetraethyl-benza-midazolocarbocyanin iodide (JC-1) staining. Upon A/R stimulation, the green fluorescence of JC-1 significantly increased, whereas the red fluorescence decreased, resulting in an elevation in the green/red fluorescence ratio. This suggests that A/R led to the decrease of MMP. Upregulation of miR-146a significantly inhibited A/R-induced reduction of MMP. The opposite result was observed in miR-146a inhibitor-treated cells (Figure 4A). Mitochondrial membrane depolarization could induce mPTP opening and subsequently lead to cytochrome *c* release from the mitochondria to the cytosol. Confocal microscopy showed that miR-146a overexpression inhibited A/R-induced decrease in fluorescence of calcein-AM, a fluorescent dye that is a sensitive indicator of mPTP opening, suggesting that miR-146a prevented the opening of mPTP (Figure 4B). In contrast, the reduction of calcein-AM fluorescence was further potentiated by miR-146a downregulation (Figure 4C). Moreover, A/R treatment increased cytochrome *c* protein expression in the cytosol; however, it decreased its expression in the mitochondria, indicating transient release of cytochrome *c*. The translocation of cytochrome *c* from the mitochondria to the cytosol was abrogated by miR-146a mimics yet promoted by the miR-146a inhibitor (Figures 4D and 4E). Furthermore, activation of caspases, a downstream event of cytochrome *c* release, was also induced by A/R stimulation, as evidenced by increased cleavage of caspase-9, caspase-3, and PARP. miR-146a overexpression inhibited, whereas miR-146a inhibition enhanced the activation of caspase-9, caspase-3, and PARP (Figure S4). Taken together, these data indicate that miR-146a ameliorates cardiomyocyte apoptosis at least partially via inhibiting the mitochondria-dependent apoptotic pathway.

miR-146a regulates cyclophilin D expression

To understand how miR-146a regulates mitochondrial dysfunction, we tested whether miR-146a influenced the expression of the mPTP complex, including voltage-dependent anion channel (VDAC), adenine nucleotide translocase (ANT), and cyclophilin D. qRT-PCR showed that overexpression of miR-146a did not alter mRNA levels of *Vdac1*, *Slc25a4*, and *Ppif* genes encoding VDAC, ANT, and cyclophilin D, respectively, in mitochondria of cardiomyocytes (Figure 5A). We then examined expression levels of these proteins in response to transfection with miR-146a mimics and found that only cyclophilin D expression was markedly decreased in cardiomyocyte mitochondria by miR-146a upregulation (Figure 5B). Notably, the other miRNAs that were downregulated upon cardiac I/R injury, as determined via microarray analysis, such as miR-535-5p, miR-330, miR-181a, and miR-34a, did not affect cyclophilin D expression (Figure S5). In addition, overexpression of miR-146a almost completely abolished A/R-induced increase in cyclophilin D expression (Figure 5C). In contrast, miR-146a knockdown significantly increased cyclophilin D protein expression; however, it did not alter its mRNA level (Figures 5D and 5E). Furthermore, RNAhybird program showed that the cyclophilin D gene coding sequence (CDS) contains a potential binding site for miR-146a (Figure 5F). Therefore, we examined the effect of miR-146a on cyclophilin D translation by using the luciferase assay. We constructed wild-type CDSs of cyclophilin D containing the binding site of miR-146a or its mutant version and cloned them into the luciferase vector. The luciferase reporter assay revealed that miR-146a decreased the translation of wild-type cyclophilin D-CDS; however, it had no distinct effect on the mutant cyclophilin D-CDS (Figure 5G). Further, the RIP results confirmed that miR-146a binds cyclophilin D in mitochondria of cardiomyocytes (Figure 5H). In addition, overexpression of miR-146a inhibited the expression of the wild-type cyclophilin D-CDS; however, it did not exert any inhibitory effect on the mutant cyclophilin D-CDS, suggesting that inhibition by miR-146a of cyclophilin D expression is binding site-dependent (Figure S6). Collectively, these results demonstrate that cyclophilin D is a specific target of miR-146a in mitochondria of cardiomyocytes.

miR-146a regulates cardiomyocyte apoptosis depending on cyclophilin D expression level

To explore whether the absence of cyclophilin D facilitated the protective effect of cardiomyocyte miR-146a against apoptosis, the cells were co-transfected with miR-146a mimics and cyclophilin D gene harboring adenovirus. The transduction efficiency of the latter

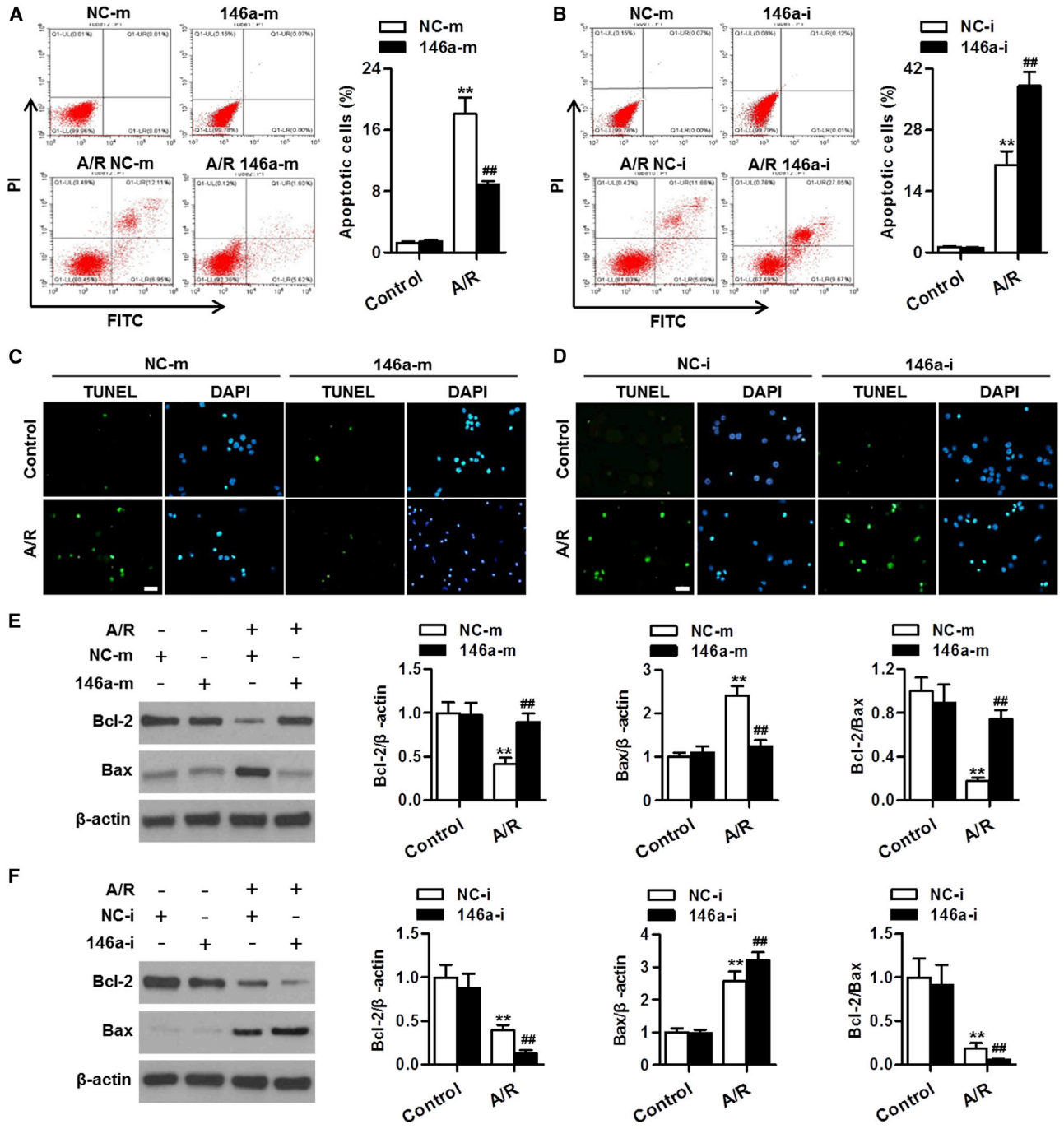

Figure 3. miR-146a mediates cardiomyocyte apoptosis induced by anoxia/reoxygenation (A/R) treatment

(A and B) Cardiomyocytes were transfected with miR-146a mimics (146a-m, 50 nmol/L, A), miR-146a inhibitor (146a-i, 50 nmol/L, B), or their corresponding negative control sequences (NC-m or NC-i) for 24 h before A/R treatment for another 48 h. Cardiomyocyte apoptosis was determined by annexin V-FITC/propidium iodide (PI) staining followed by flow cytometry. (C and D) TUNEL (green) and DAPI (blue) staining of cardiomyocytes treated with miR-146a mimics (C) or miR-146a inhibitor (D) under A/R conditions. (E and F) Changes in expression levels of Bcl-2 and Bax proteins in cardiomyocytes treated with miR-146a mimics (E) or miR-146a inhibitor (F) after A/R stimulation. Representative western blot images are shown in leftmost panels. Bar charts represent densitometric analysis data of relative levels of Bcl-2, Bax, and Bcl-2/Bax ratio. $^{**}p < 0.01$ versus NC-m control or NC-i control; $^{\#\#}p < 0.01$ versus NC-m A/R or NC-i A/R, n = 6–8.

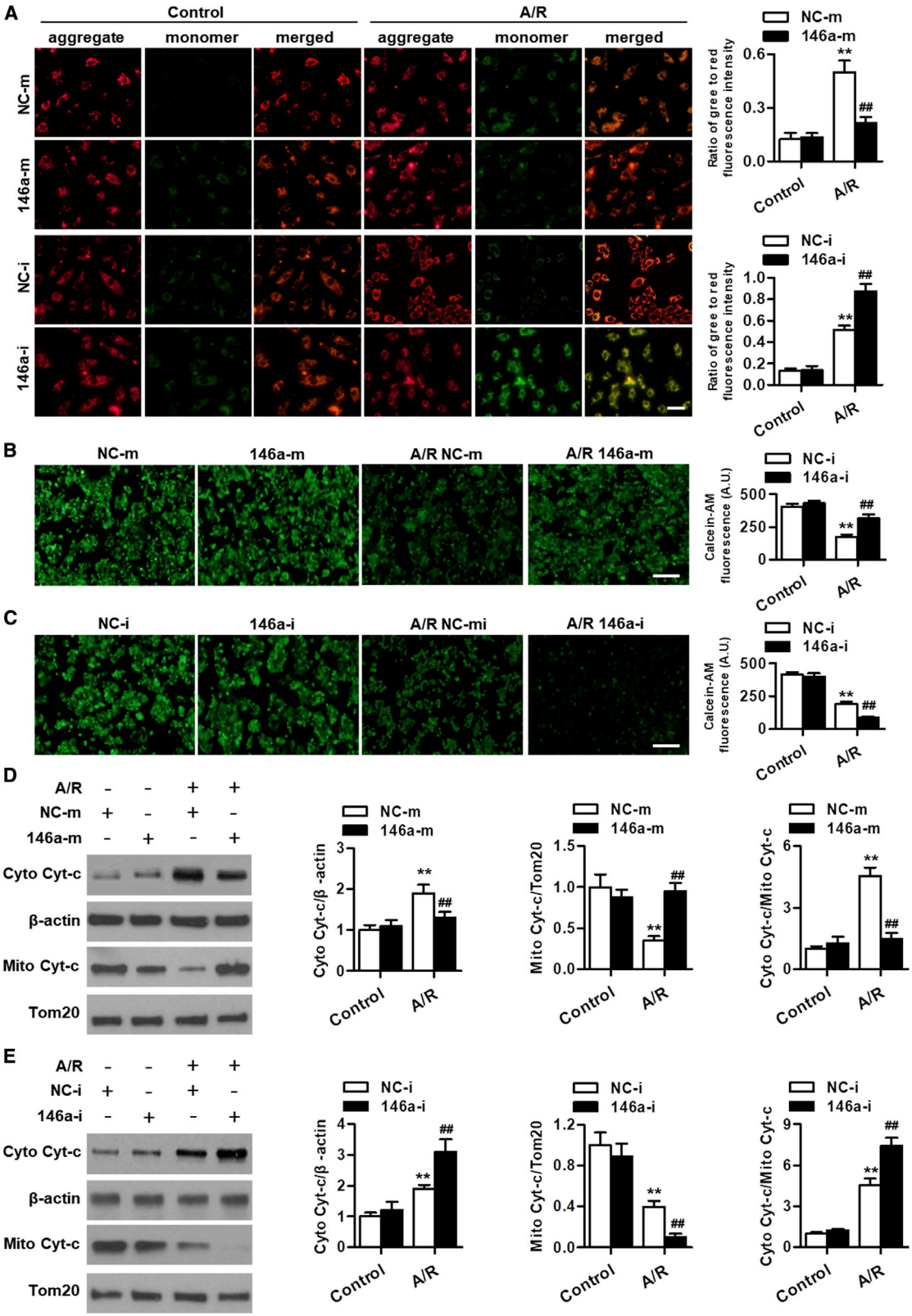

(legend on next page)

adenovirus was confirmed by the increased expression of cyclophilin D (Figure S7). Under A/R conditions, the inhibitory effects of miR-146a overexpression on cardiomyocyte apoptosis were largely reversed by the transduction with Ad-CypD (Figures 6A and 6B). Ad-CypD markedly blunted the increase of Bcl-2 expression and Bcl-2/Bax ratio in cells treated with miR-146a mimics and increased Bax expression after A/R challenge (Figure 6C). Moreover, restoration of cyclophilin D expression abolished the regulatory effects of miR-146a overexpression on A/R-induced cleavage of caspase-9, caspase-3, and PARP (Figure 6D). These data indicate that cyclophilin D was required for miR-146a-mediated inhibition of cardiomyocyte apoptosis following A/R challenge.

Cyclophilin D deficiency abolishes aggravating effects of miR-146a deficiency on cardiac I/R injury

We crossed miR-146a^{CKO} mice with *Ppif*^{CKO} mice (miR-146a^{CKO}*Ppif*^{CKO}) to examine the requirement for cyclophilin D in cardiac I/R injury induced by miR-146a deficiency *in vivo* (Figure S8). The infarct size was consistently lower in miR-146a$^{f/f}$ mice and miR-146a^{CKO} mice after cardiomyocyte-specific knockout of cyclophilin D (Figures 7A and 7B). The increase in LDH level caused by miR-146a deficiency under A/R conditions was also markedly inhibited in miR-146a^{CKO}PPIF^{CKO} mice (Figure 7C). Furthermore, the lack of cyclophilin D largely abolished the exacerbation of cardiac function impairment that was observed in mice with cardiomyocyte-specific knockout of miR-146a (Figures 7D and 7E). In addition, the increase in cardiomyocyte apoptosis in the myocardium of miR-146a^{CKO} mice was almost completely reversed by cyclophilin D knockout (Figures 7F and 7G). Thus, upregulation of cyclophilin D may underlie the deleterious effects of miR-146a deficiency on cardiac I/R injury.

DISCUSSION

In this study, we reveal a novel role of miR-146a in cardiomyocyte apoptosis and cardiac I/R injury. We provide evidence that miR-146a localizes in the mitochondria and modulates the expression of cyclophilin D, thereby regulating mPTP opening and mitochondria-dependent apoptotic pathway in cardiomyocytes.

Over the past few years, many studies have indicated that various miRNAs regulate myocardial infarction due to I/R injury in ischemic heart diseases.[7,10] Alteration in miRNA expression may serve as a causal factor in the development of cardiac I/R injury. For example, the levels of miRNAs from the miR-15 family were increased under cardiac I/R injury, which directly promoted myocardial infarction.[15] Inhibition of miR-15 ameliorated cardiac I/R injury by regulating mitochondrial function and apoptosis.[15,16] In contrast, miR-499 and miR-214 were increased in myocardial infarction, and this increase had a protective effect,[17,18] indicating that the upregulation of miR-499 and miR-214 is likely a compensatory protection rather than a pathogenic phenomenon. Thus, it is not surprising that miRNA-based therapeutics are considered promising for treatment of ischemic disease.[19] Notably, a large body of work has focused on the major role of these miRNAs commonly present in the cytosol of cells, where they regulate protein synthesis or degradation by affecting nuclear genes.[10,19] The information about the role of mitochondrial miRNAs in regulating mitochondrial gene expression and mitochondrial function is limited, although several recent studies have shown the presence of miRNAs in the mitochondria.[4,7,10]

Recently, some mitochondrial miRNAs have been found to be differentially expressed during myocardial infarction and heart failure, suggesting a role of mitochondrial miRNAs in the regulation of cardiac function.[4,7,20] In a study by Yan et al.,[4] miR-762 was found to be localized in the mitochondria of cardiomyocytes, where its level increased under A/R conditions, which contributed to decreased mitochondrial complex I enzyme activity and increased levels of reactive oxygen species and cell apoptosis. Moreover, mature miR-181c was predominantly expressed in the mitochondria, where it likely regulated mitochondrial genes and generation of reactive oxygen species, which could lead to mitochondrial dysfunction.[7] In the present study, by using the miRNA microarray assay, we found that miR-146a was significantly decreased in the mitochondrial fractions of ischemic heart; however, it was not altered in the cytosolic fraction. In addition to previous studies that reported an abundance of miR-146a in the heart,[13] our results further extended this notion by showing that miR-146a was nearly threefold more abundant in the mitochondria than in the cytosol. To the best of our knowledge, this is the first demonstration of the presence of miR-146 in the mitochondria, as well as of the alterations of miR-146a levels in cardiomyocyte mitochondria in response to cardiac I/R injury. These findings, therefore, indicate a crucial role of mitochondrial miR-146a in ischemic heart disease. Further experiments revealed that specific knockout of miR-146a in cardiomyocytes aggravated cardiac I/R injury and dysfunction. These observations were consistent with the protective role of miR-146a in heart diseases, such as myocardial infarction, fibrosis, and doxorubicin cardiotoxicity.[12,13,21]

Another significant finding of our study was the demonstration of miR-146a synthesis in the nucleus and subsequent translocation

Figure 4. miR-146a ameliorates A/R-induced mitochondrial dysfunction in cardiomyocytes

(A) Cardiomyocytes were treated with miR-146a mimics or miR-146a inhibitor for 24 h prior to A/R stimulation for 48 h and then with AngII (10 μM) for another 24 h. Mitochondrial membrane potential was measured using JC-1 staining. Representative images of JC-1-derived fluorescence in cardiomyocytes are shown in the left panel. JC-1 aggregate image displays red fluorescence, JC-1 monomer image displays green fluorescence, and the merged image combines red and green fluorescence images. Quantitative analysis of the green/red fluorescence ratio is provided in the right panel. (B and C) Opening of mitochondrial permeability transition pore in cardiomyocytes treated with miR-146a mimics (B) or miR-146a inhibitor (C) under A/R conditions was detected by calcein-AM staining. (D and E) Cytochrome *c* protein expression in the cytosol and mitochondria was determined by western blot. Transfection with miR-146a mimics inhibited the release of cytochrome *c* into the cytosol (D), whereas miR-146a inhibitor promoted the release of cytochrome *c* (E). Mitochondrial marker protein Tom20 was used as an internal control. $^{**}p < 0.01$ versus NC-m control or NC-i control; $^{\#\#}p < 0.01$ versus NC-m A/R or NC-i A/R, n = 6–8.

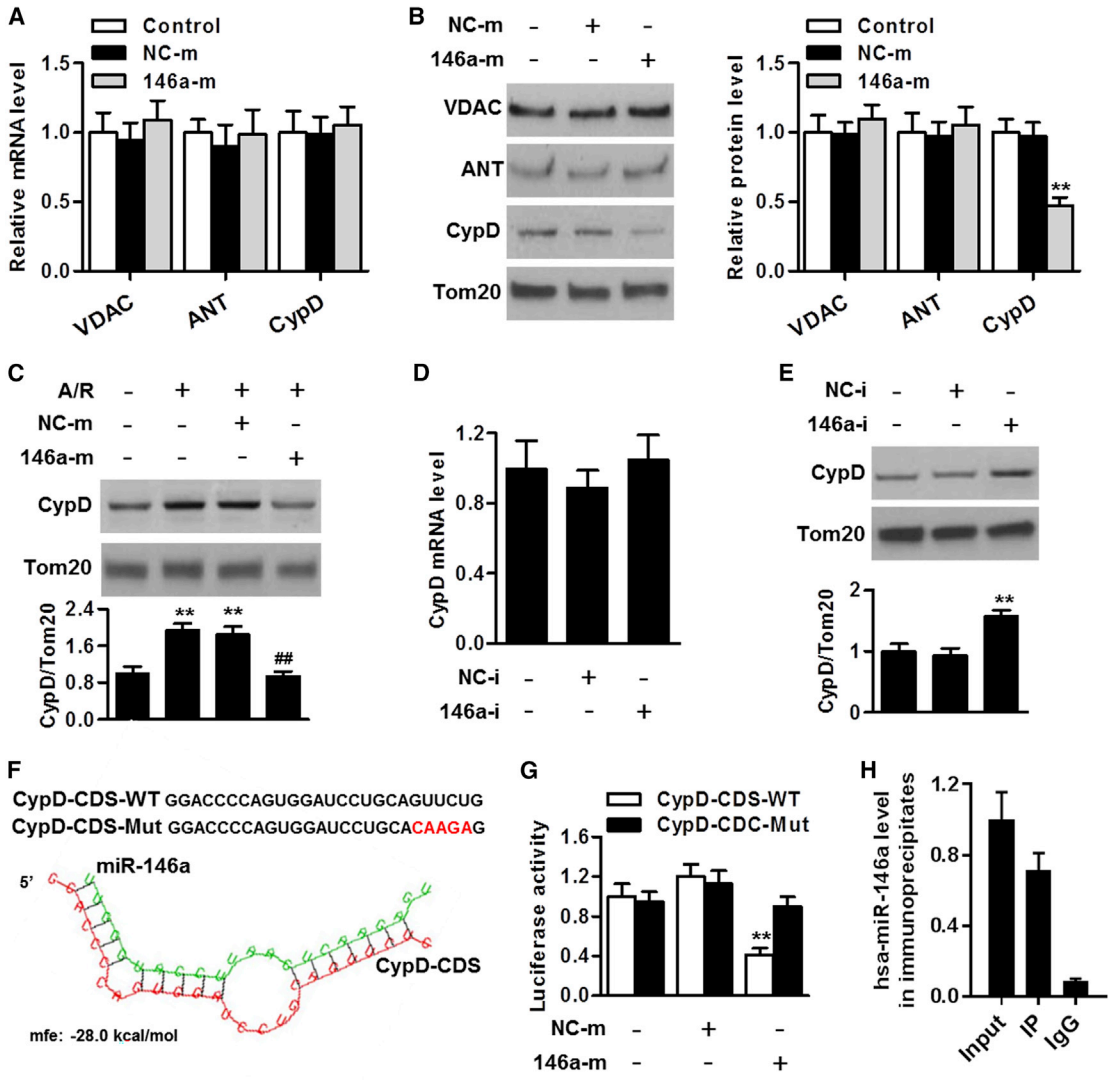

Figure 5. miR-146a regulates cyclophilin D expression

(A) qRT-PCR analysis of mRNA expression of the *Vdac1*, *Slc25a4*, and *Ppif* genes encoding voltage-dependent anion channel (VDAC), adenine nucleotide translocase (ANT), and cyclophilin D (cyclophilin D), respectively, in cardiomyocyte mitochondria after transfection with miR-146a mimics for 48 h (n = 5). (B) miR-146a upregulation decreased cyclophilin D protein expression in mitochondria; however, it had no distinct effect on expression levels of VDAC and ANT. **p < 0.01 versus control, n = 6. (C) Cardiomyocytes were pretreated with miR-146a mimics before A/R stimulation. Western blot analysis of cyclophilin D protein expression in the mitochondrial fraction is shown. **p < 0.01 versus control; ##p < 0.01 versus A/R, n = 6. (D and E) Cyclophilin D mRNA (D) and protein (E) expression levels in cardiomyocyte mitochondrial fraction treated with miR-146a inhibitor for 48 h. **p < 0.01 versus control, n = 6. (F) Analysis of *Ppif* (cyclophilin D) gene coding sequence (CDS) region for the potential binding site of miR-146a. (G) miR-146a inhibits *Ppif* (cyclophilin D) translation by binding to its CDS. Cardiomyocytes were co-transfected with the luciferase construct carrying wild-type cyclophilin D-CDS (cyclophilin D-CDS-WT) or mutated cyclophilin D-CDS (cyclophilin D-CDS-Mut) and miR-146a mimics or mimics negative control, whereupon the cells were harvested for the measurement of luciferase activity. **p < 0.01 versus control, n = 6. (H) qRT-PCR analysis of miR-146a levels in the cyclophilin D immunoprecipitate obtained from the cardiomyocyte mitochondrial fraction (n = 4).

from the cytosol into the mitochondria instead of originating from mitochondrial genome-derived mRNA molecules. The biogenesis of miRNA commonly takes place by multiple steps in both the nucleus and cytosol.[22] First, miRNAs are transcribed from genes to produce primary miRNA (pri-miRNA) by RNA polymerase II in the nucleus. Then, pri-miRNA with the stem-loop structure is modified and cleaved by Drosha to form pre-miRNA with the hairpin-loop structure, followed by the export from the nucleus to cytosol. Finally, mature miRNAs are generated in the cytosol after pre-miRNAs originated from the nucleus are processed by dicer. In the present study, we found that the relative level of nuclear or mitochondrial miR-146a remained far below the relative level in the whole heart, suggesting that pre-miR-146a is present predominantly in the cytosol and originally derives from the nucleus. This concurs with the discoveries that

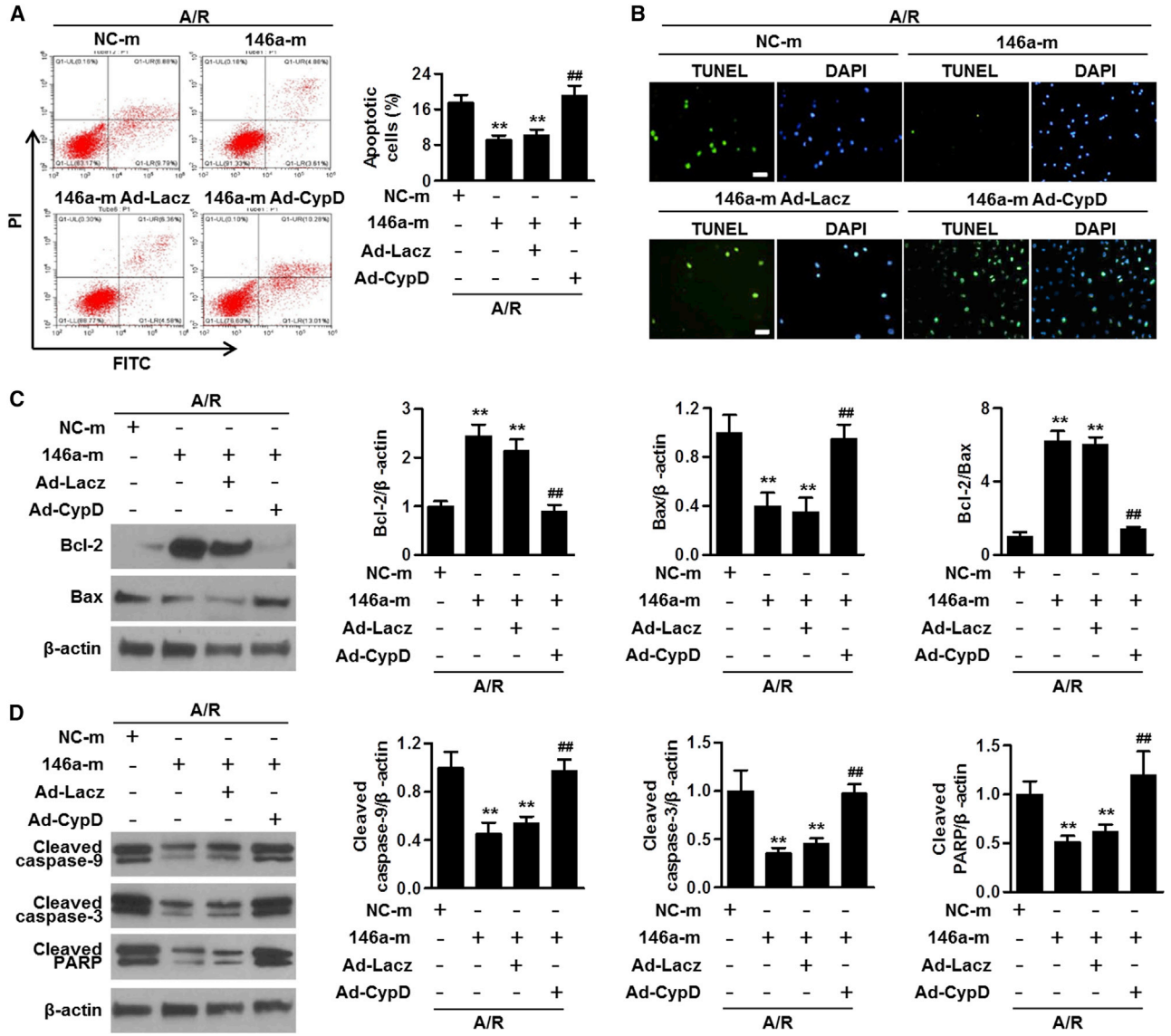

Figure 6. Cyclophilin D is involved in the regulation of cardiomyocyte apoptosis by miR-146a

(A) Cardiomyocytes were transfected with miR-146 mimics and simultaneously transduced with adenoviruses carrying either Lacz (Ad-Lacz) or cyclophilin D (Ad-CypD) encoding constructs for 24 h before A/R stimulation. Cardiomyocyte apoptosis was determined by annexin V-FITC/PI staining using flow cytometry. (B) TUNEL staining of cardiomyocytes treated as described above. (C and D) Western blot analysis of Bcl-2, Bax (C), cleaved caspase-9, cleaved caspase-3, and cleaved PARP protein expression levels (D). Representative western blot images are shown in the leftmost column. Bar charts illustrate results of the densitometric analysis. $^{**}p < 0.01$ versus NC-m A/R; $^{\#\#}p < 0.01$ versus 146a-m A/R, n = 4–7.

miR-181c and 5S rRNA reside in the mitochondria after being translocated from the cytosol.[7,23] However, it should be noted that the mitochondria is not an autonomous organelle but rather communicates with the nucleus through retrograde signaling.[24,25] This suggests that other small molecules involved in the crosstalk between the nucleus and mitochondria may also play a role in the deregulation of mitochondrial miRNA levels.[24] Thus, the mechanisms underpinning mitochondrial miRNA deregulation in response to I/R injury appear to be complex, warranting further investigation.

It has been well established that irreversible myocardial apoptosis occurs throughout the entire process of cardiac I/R injury and remodeling.[2,26,27] The degree of myocardial apoptosis is closely associated with therapeutic outcome and prognosis of myocardial infarction.[19,28] Herein, we showed that cardiomyocyte miR-146a deficiency significantly exacerbated I/R-induced myocardial apoptosis. This result is consistent with previous study that used a doxorubicin cardiotoxicity model.[12] Data from that study together with our present findings further support the protective role of miR-146a against

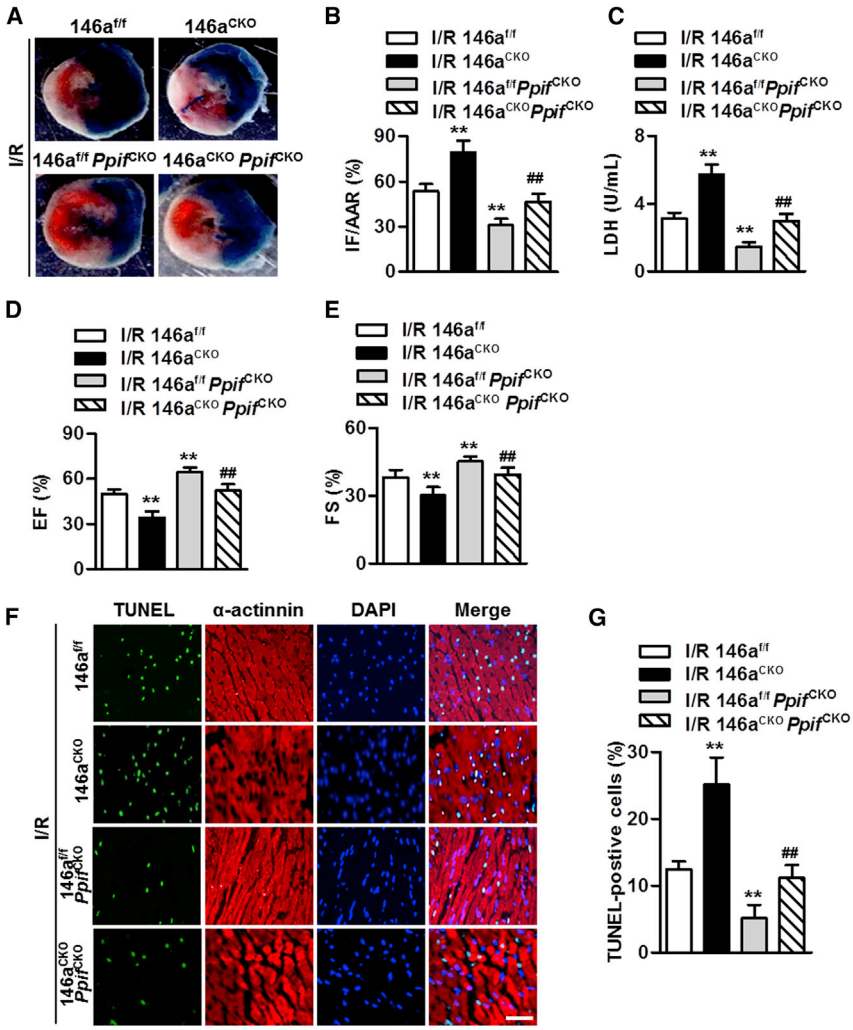

Figure 7. Cardiomyocyte miR-146a regulates cardiac I/R injury in a cyclophilin D-dependent manner

(A and B) miR-146a$^{f/f}$/MHC-Cre mice (miR-146a^{CKO}) were crossed with *Ppif*$^{f/f}$/MHC-Cre mice (*Ppif*^{CKO}) to obtain miR-146a^{CKO}*Ppif*^{CKO} mice and underwent I/R surgery. Myocardial infarct was visualized by Trypan blue (A) and 2,3,5-triphenyltetrazolium chloride staining and assessed as the ratio of infarcted area (IF) to area at risk (AAR) (IF/AAR) (B). **p < 0.01 versus I/R 146a$^{f/f}$; ##p < 0.01 versus I/R 146a^{CKO}, n = 6 per group. (C) Measurements of LDH serum levels. **p < 0.01 versus I/R 146a$^{f/f}$; ##p < 0.01 versus I/R 146a^{CKO}, n = 10 per group. (D and E) Analysis of echocardiographic left ventricular ejection fraction (EF, D) and percentage fractional shortening (FS, E) data at the end of 24 h reperfusion. **p < 0.01 versus I/R 146a$^{f/f}$; ##p < 0.01 versus I/R 146a^{CKO}, n = 8 per group. (F) Representative images of myocardial tissue sections stained with TUNEL and anti-α-actinin antibody. (G) QuantiGication of apoptotic cardiomyocytes in each group. **p < 0.01 versus I/R 146a$^{f/f}$; ##p < 0.01 versus I/R 146a^{CKO}, n = 6 per group.

myocardial apoptosis. Given the importance of mitochondria in the regulation of cell apoptosis and the localization of miRNA-146a in mitochondria, we examined the influence of miR-146a on the mitochondrial function and related apoptotic pathway in cardiomyocytes. Upon apoptotic stimuli, the pro-apoptotic proteins (e.g., Bax) translocate to the mitochondrial membrane and abolish the effect of anti-apoptotic proteins (e.g., Bcl-2) to maintain cell survival.[6,29] The disruption of the Bcl2-Bax balance induces MMP depolarization and mitochondrial membrane permeabilization via the formation and opening of mPTP, followed by leakage of cytochrome *c* from the mitochondria and activation of caspases.[8,9] In the present study, miR-146a downregulation dramatically potentiated the activation of the mitochondria-dependent apoptotic pathway, whereas miR-146a overexpression effectively attenuated mitochondrial dysfunction.

Another novel finding of this study was the RIP assay evidence for the presence of miR-146a and Ago2 complex in the mitochondria. Ago2 is the only catalytically active member of the Ago family (Ago1–4) and the main component of RNA-induced silencing complex (RISC).[30] Moreover, it facilitates the translocation of miRNAs into the mitochondria by binding to the RISC in the cytosol.[31] Given that Ago2 was shown to be enriched in the mitochondria,[4,7,32] our results not only further confirm the presence of miR-146a in the mitochondria but also suggest that miR-146a forms a functional RISC that mediates targeted mRNA translation and degradation. The opening of mPTP is thought be critical for the initiation of MMP depolarization and subsequent mitochondrial dysfunction, leading to cell apoptosis.[9] Cyclophilin D, ANT, and VDAC have been identified as the components of the mPTP complex.[33] In an attempt to explore the mechanisms of miRNA-146a effects in the mitochondria, we determined how mitochondrial miR-146a modulated expression levels of these proteins. Intriguingly, we found that cyclophilin D expression in the mitochondria, not that of ANT or VDAC, was decreased by miR-146a overexpression, suggesting that mitochondrial miR-146a regulates mPTP opening in a cyclophilin D-dependent manner. Further, miR-146a dramatically inhibited cyclophilin D protein without affecting its mRNA expression in mitochondria, indicating that miR-146a suppresses cyclophilin D protein expression by the Ago2-mediated translation repression mechanism. Of importance, I/R damage is known to be attenuated in cyclophilin D knockout mice (*Ppif*$^{-/-}$) in many models.[34–36] Our results showed that overexpression of cyclophilin D reversed the inhibitory effect of miR-146a on mitochondria-dependent apoptosis in cardiomyocytes and that the lack of cyclophilin D in cardiomyocytes minimized the deleterious effects of miR-146a deficiency on myocardial infarction and apoptosis. These data are consistent with a previous study that demonstrated a positive effect of cyclophilin D deficit in the amelioration of ischemic heart disease.[34]

It should be noted that miRNAs are complex regulators that target multiple genes or entire pathways rather than a single gene. Therefore, it remains possible that, although the results of the luciferase reporter and RIP experiments suggest that miR-146a directly binds cyclophilin D, the regulation of miR-146a on cyclophilin D expression may results from indirect effects. In addition to miR-146a, several miRNAs are also dysregulated in mitochondria upon cardiac I/R injury, such as miR-535-5p, miR-330, miR-181a, and miR-34a. These results, together with previous studies showing other aberrant miRNAs during cardiac I/R injury, suggest that although the miR-146a-cyclophilin D axis is an important mechanism underlying cardiomyocyte apoptosis and myocardial infarction, it does not represent the only associated mechanism. We therefore plan to investigate the role of miRNA networks in cardiac I/R injury in future studies.

Our study unveiled the role of mitochondrial miR-146a in cardiomyocyte apoptosis and provided novel mechanistic insights into the effects of miR-146a on myocardial infarction.

MATERIALS AND METHODS

Reagents

TRIzol, fetal bovine serum (FBS), Dulbecco's modified Eagle's medium (DMEM), penicillin-streptomycin solution, Lipofectamine 2000, JC-1 dye, IgG-Alexa Fluor 594 secondary antibody, 4′,6-diamidino-2-phenylindole (DAPI), calcein-AM, and protease inhibitor cocktail were obtained from Invitrogen (Carlsbad, CA, USA). miR-146a mimics, mimics negative control, miR-146a inhibitor, inhibitor negative control, as well as adenovirus vectors carrying genes encoding cyclophilin D (Ad-CypD) and Lacz (Ad-Lacz) were purchased from Sunbio Medical Biotechnology (Shanghai, China). Unless otherwise indicated, all other chemicals were purchased from Sigma-Aldrich (St. Louis, MO, USA).

Animals

All animal experiments were conducted in strict accordance with the Guidelines for the Care and Use of Laboratory Animals and approved by the Animal Ethics Committee of the Guilin Medical University (Guangxi, China). Littermate miR-146a$^{flox/flox}$ mice (miR-146a$^{f/f}$) were obtained from the Jackson Laboratory (stock number: 034343; Bar Harbor, ME, USA) and used as control animals. Cardiomyocyte miR-146a-deficient mice (miR-146a^{CKO}) were produced by crossing miR-146a$^{f/f}$ mice with MHC-Cre mice (B6.FVB-Tg(*Myh6*-cre) 2182Mds/J; stock number: 011038; Jackson Laboratory) to generate miR-146a$^{f/f}$/MHC-Cre mice. Cardiomyocyte-specific cyclophilin D knockout mice (*Ppif*^{CKO}) were generated by mating *Ppif*$^{flox/flox}$ mice (*Ppif*$^{f/f}$, stock number: 005737; Jackson Laboratory) with MHC-Cre mice, in which exons 3–5 of the *Ppif* gene encoding mitochondrial cyclophilin D were flanked by two loxP sites. miR-146a^{CKO}*Ppif*^{CKO} mice were generated by breeding miR-146a$^{f/f}$/MHC-Cre mice with *Ppif*$^{f/f}$/MHC-Cre mice. The animals were genotyped by using PCR analysis of tail genomic DNA using specific primers (Table S1). All animals were maintained in individual ventilated cages with controlled temperature and humidity under a 12/12-h day/night cycle. Standard chow and tap water were available *ad libitum*.

Cardiac I/R model

The cardiac I/R model was established in 8-week-old male mice following a previously described protocol.[15] Briefly, the mice were anesthetized with pentobarbital sodium (40 mg/kg), and, following thoracotomy, the left main descending coronary artery at 2 to 3 mm from the tip of the left auricle was sutured and tied with a slip knot. After 30 min of ischemia, the slip knot was released gradually, followed by reperfusion for 4 h (for biochemical and apoptosis assays) and for 24 h (for cardiac function tests). Sham-operated mice underwent the same surgical procedures for suture tying.

Mitochondrial fraction isolation

Freshly isolated mitochondria were prepared from the hearts or from cultured cardiomyocytes using a Mammalian Mitochondria Isolation Kit (Biovision, Exton, PA, USA) according to the protocols provided by the manufacturer.

qRT-PCR

Total RNA and miRNA-enriched RNA were isolated from whole hearts and mitochondrial fractions using an RNAeasy Kit (QIAGEN, Venlo, the Netherlands) and a MirVana miRNA Isolation Kit (Thermo Fisher Scientific, Waltham, MA, USA), respectively. Stem-loop qRT-PCR for miRNA levels was performed on a 7500 Fast Real-Time PCR System (Applied Biosystems, Carlsbad, CA, USA) using specific Taqman assays for miRNA and specific primers (Applied Biosystems). qPCR was performed with a Fast SYBR Green Master Mix Kit (Applied Biosystems) to determine mRNA expression of *Vdac1*, *Slc25a4*, and *Ppif* genes encoding VDAC, ANT, and cyclophilin D proteins, respectively. The levels of mRNAs and miRNAs were quantified by using the $2^{(-\Delta\Delta ct)}$ method and normalized by the levels of U6, 12S rRNA, or *Gapdh* RNA. The primer sequences for qPCR are listed in Table S2.

microRNA profiling

Mitochondrial RNA was isolated from mouse hearts at 4 h post I/R operation by TRIzol and used for GeneChip miRNA 1.0 arrays (Santa Clara, CA, USA) according to the protocol recommended by the manufacturer. Labeled miRNA was hybridized to Affymetrix miRNA 1.0 array, and the stained array was scanned using an Affymetrix GeneChip Scanner 3000. The differentially expressed genes were revealed by using R package limma with cutoff values for fold-change >1.5 and $p < 0.05$.

RIP

The RIP assay was performed using a Magna RIP kit (Millipore, Billerica, MA, USA). The mitochondrial fraction was lysed with RIP lysis buffer. After centrifugation, the supernatant was incubated with an anti-Argonaute 2 (anti-Ago2) antibody (Abcam, Cambridge, MA, USA) or normal IgG antibody (Cell Signaling Technology, Billerica, MA, USA) overnight at 4°C. Then, A/G magnetic beads were added to the samples and incubated at 4°C for 4 h. The beads were harvested using a magnetic separator (Millipore) and used to isolate RNA with PCA reagent (phenol:chloroform:isoamyl alcohol at a ratio of 125:24:1). The isolated RNA was subjected to qRT-PCR analysis.

Cell culture, transfection, transduction, and treatment

AC16 cardiomyocytes were obtained from the American Tissue Type Collection (ATCC, Manassas, VA, USA) and cultured in DMEM supplemented with 10% FBS, 1% penicillin-streptomycin solution in a humidified incubator in the atmosphere of 95% air and 5% CO_2 at 37°C. The cells were starved in FBS-free medium for 12 h and then transfected with miR-146a mimics, miR-146a inhibitor, or their corresponding negative controls for 24 h using Lipofectamine 2000 in accordance with the manufacturer's instructions. To restore the expression of cyclophilin D, cardiomyocytes were transfected with miR-146a mimics and simultaneously transduced with Ad-CypD or Ad-Lacz for 24 h. Afterward, the culture medium was replaced by FBS-free medium saturated with 95% N_2/5% CO_2 at an incubator with 95% N_2/5% CO_2 gas supply for 24 h. Then the culture medium was further changed to the medium containing 10% FBS in a humidified incubator containing 95% air and 5% CO_2 for another 24 h.

Fluorescence *in situ* hybridization

Cardiomyocytes were fixed with acid/methanol and allowed to dry overnight. Then, the cells were hybridized *in situ* with the probe for miR-146a (40 nmol/L double-DIG LNA microRNA probe, Exiqon, Copenhagen, Denmark) for 1 h at 37°C in the presence of proteinase K, which facilitated hybridization of DIG-labeled LNA probes with the miRNA sequence. Subsequently, the cells were stained with the MMP dye MitoTracker Red for 30 min in the absence of proteinase K. After a series of washes with phosphate-buffered saline (PBS), fluorescence was observed by a laser scanning confocal microscope (OLS5000, Olympus, Tokyo, Japan).

ATP assay

ATP synthesis was determined using an ATP colorimetric assay kit (Biovision, Milpitas, CA, USA). Cells were collected, and the assay was performed in 96-well plates according to the manufacturer's instructions. The optical density (OD) value was obtained at 570 nm using a micro-plate reader (Bio-Tek, Winooski, VT, USA). The concentration of ATP was calculated according to the standard curve.

Infarct size measurement

Myocardial infarct size was measured as described previously.[4,15] Four hours after reperfusion, the left anterior descending coronary artery was retied, and 2 mL of 0.6% Trypan blue was injected into the ascending aorta to define the non-ischemic area. The hearts were excised immediately and kept at −20°C overnight. Then, the left ventricle was sliced into 2-mm-thick sections and incubated with 1% 2,3,5-triphenyltetrazolium chloride (TTC) for 15 min at 37°C to define the ischemic area (area at risk, AAR). The areas without Trypan blue and TTC staining represented infarcted (IF) myocardium. Infarct size was expressed as infarct area divided by AAR (IF/AAR).

LDH assay

Blood samples for LDH measurements were harvested 4 h after reperfusion and centrifuged for 10 min at 3,000 × *g* to obtain serum. LDH level was measured by a CytoTox 96 Non-Radioactive Cytotoxicity Assay kit (Promega, Madison, WI, USA) according to the manufacturer's protocols.

Echocardiographic analysis

Echocardiograms were obtained at the end of the 4 h reperfusion period using a high-resolution ultrasound imaging system (Panoview β1500, Cold Spring Biotech, Beijing, China) in anesthetized mice (1.5% isoflurane). The left ventricular EF and FS data were calculated using the accompanying software by a single observer blinded to the group assignment.

TUNEL staining

Cardiomyocyte apoptosis was detected by TUNEL staining, as previously described.[4,12,17] The frozen sections of the left ventricle front wall (LVFW) were initially incubated with an anti-α-actinin antibody (1:100 dilution; Santa Cruz, CA, USA) overnight at 4°C, followed by the incubation with goat anti-mouse IgG-Alexa Fluor 594 (1:500 dilution) for 1 h. After washing with PBS, the sections were incubated with TUNEL reagent (Roche, Mannheim, Germany) for 1 h at 37°C. For *in vitro* experiments, cardiomyocytes were fixed with 4% paraformaldehyde and incubated with TUNEL reagent for 1 h. The nuclei were counterstained with DAPI. Apoptotic cells were observed and captured by a laser scanning confocal microscope (OLS5000).

Apoptosis analysis

Cardiomyocyte apoptosis was evaluated by flow cytometry (CytoFLEX; Beckman Coulter, Brea, CA, USA) using an Annexin V-FITC/PI Apoptosis Detection Kit (BD Biosciences, San Diego, CA, USA) following the manufacturer's protocols. The percentage of cells undergoing apoptosis was determined with the accompanying software.

Western blot

Cardiomyocyte LVFW samples were lysed using RIPA lysis buffer (Beyotime Institute of Biotechnology, Jiangsu, China) supplemented with protease inhibitor cocktail and centrifuged at 10,000 × *g* for 15 min. Protein content of samples was determined by the Bradford assay (Bio-Rad Laboratories, Carlsbad, CA, USA). Aliquots of each sample were separated in a 12% Tris/glycine sodium dodecyl sulfate/polyacrylamide gel and then transferred onto a nitrocellulose membrane that was blocked with skimmed milk for 1 h. The membranes were respectively probed overnight at 4°C with antibodies against the following proteins: Bcl-2 (1:1,000 dilution), Bax (1:1,000 dilution), cytochrome *c* (1:500 dilution), caspase-9 (1:1,000 dilution), caspase-3 (1:500 dilution), PARP (1:1,000 dilution), and ANT (1:200 dilution) (Cell Signaling Technology); β-actin (1:2,000 dilution), TOM20 (1:500 dilution), and VDAC (1:500 dilution) (Santa Cruz); and cyclophilin D (1:100 dilution; Millipore). After washing with Tris-buffered saline-Tween (TBS-T) buffer three times, the membranes were incubated with appropriate horseradish peroxidase-conjugated secondary antibodies (Beyotime Institute of Biotechnology) for 1 h, and the bound proteins were detected with an enhanced chemiluminescence kit (Thermo Fisher Scientific). The blots were scanned and quantified using ImageJ program (NIH, Bethesda, MD, USA).

Measurement of MMP

MMP was measured by JC-1 dye as previously described.[6] Cardiomyocytes were transfected with miR-146a mimics, miR-146a inhibitor, or their negative controls and then subjected to the A/R treatment. Afterward, the cells were incubated with JC-1 working solution in a dark room at 37°C for 15 min and observed by a laser scanning confocal microscope (OLS5000). Red fluorescence represented potential-dependent accumulation in the mitochondria of healthy cells, whereas green fluorescence indicated leakage of the monomeric dye into the cytoplasm and MMP breakdown. Consequently, MMP change was expressed as the ratio of green to red fluorescence.

mPTP opening assay

mPTP opening in cardiomyocytes was detected by calcein-AM staining. The cells were incubated with 1 μmol/L calcein-AM and 1 μmol/L $CoCl_2$ under the A/R condition for 24 h. Calcein-AM fluorescence was captured by a laser scanning confocal microscope (OLS5000). The reduction of the mitochondrial calcein-AM signal reflected the opening of mPTP.

Luciferase activity assay

Genomic DNA was extracted from cardiomyocytes using a Genomic DNA Extraction Kit (QIAGEN). The cyclophilin D gene CDS was amplified using PCR and then inserted downstream of the stop codon of the pGL3-basic luciferase reporter vector. Cyclophilin D-CDS mutant was constructed by mutating the putative miR-146a binding site using a QuikChange Lightning Site-Directed Mutagenesis Kit (Agilent Technologies, Beijing, China) based on the template of wild-type cyclophilin D-CDS. Cardiomyocytes were transfected with miR-146a mimics in combination with wild-type or mutant cyclophilin D-CDS using Lipofectamine 2000. Additionally, Renilla luciferase control pRL-TK vector (Promega, Madison, WI, USA) was also co-transfected as endogenous control. Luciferase activity was assessed using a Dual-Luciferase Reporter Assay System (Promega) and normalized to Renilla luciferase activity.

Statistical analysis

Results are presented as the mean ± standard error of mean (SEM). To compare individual datasets between two groups, the Student's t test was performed. One-way analysis of variance with post hoc Bonferroni's correction was used for comparisons of more than two groups. Differences were considered statistically significant when $p < 0.05$. Statistical evaluation was performed by using SPSS 17.0 software (SPSS, Chicago, IL, USA).

SUPPLEMENTAL INFORMATION

Supplemental information can be found online at https://doi.org/10.1016/j.omtn.2021.01.034.

ACKNOWLEDGMENTS

This work was supported by the National Natural Science Foundation of China (grant no. 81960079) and Guangxi BaGui Scholars Special Project.

AUTHOR CONTRIBUTIONS

Data curation, Q.S.; writing – original draft preparation, Q.S.; investigation, Q.S., X.Y.; supervision, Q.S.; writing – review & editing, Q.S.; conceptualization, Y.X.; methodology, Y.X., Y.L.; software, Y.X., Y.L.; visualization, X.Y.; validation, Y.L.

DECLARATION OF INTERESTS

The authors declare no competing interests.

REFERENCES

1. Kuhn, T.C., Knobel, J., Burkert-Rettenmaier, S., Li, X., Meyer, I.S., Jungmann, A., Sicklinger, F., Backs, J., Lasitschka, F., Muller, O.J., et al. (2020). Secretome Analysis of Cardiomyocytes Identifies PCSK6 (Proprotein Convertase Subtilisin/Kexin Type 6) as a Novel Player in Cardiac Remodeling After Myocardial Infarction. Circulation *141*, 1628–1644.
2. Cannon, R.O., 3rd (2005). Mechanisms, management and future directions for reperfusion injury after acute myocardial infarction. Nat. Clin. Pract. Cardiovasc. Med. *2*, 88–94.
3. Muzumdar, R.H., Huffman, D.M., Calvert, J.W., Jha, S., Weinberg, Y., Cui, L., Nemkal, A., Atzmon, G., Klein, L., Gundewar, S., et al. (2010). Acute humanin therapy attenuates myocardial ischemia and reperfusion injury in mice. Arterioscler. Thromb. Vasc. Biol. *30*, 1940–1948.
4. Yan, K., An, T., Zhai, M., Huang, Y., Wang, Q., Wang, Y., Zhang, R., Wang, T., Liu, J., Zhang, Y., et al. (2019). Mitochondrial miR-762 regulates apoptosis and myocardial infarction by impairing ND2. Cell Death Dis. *10*, 500.
5. Zhu, J., Yao, K., Wang, Q., Guo, J., Shi, H., Ma, L., Liu, H., Gao, W., Zou, Y., and Ge, J. (2016). Ischemic Postconditioning-Regulated miR-499 Protects the Rat Heart Against Ischemia/Reperfusion Injury by Inhibiting Apoptosis through PDCD4. Cell. Physiol. Biochem. *39*, 2364–2380.
6. Liu, X.Y., Zhang, F.R., Shang, J.Y., Liu, Y.Y., Lv, X.F., Yuan, J.N., Zhang, T.T., Li, K., Lin, X.C., Liu, X., et al. (2018). Renal inhibition of miR-181a ameliorates 5-fluorouracil-induced mesangial cell apoptosis and nephrotoxicity. Cell Death Dis. *9*, 610.
7. Das, S., Ferlito, M., Kent, O.A., Fox-Talbot, K., Wang, R., Liu, D., Raghavachari, N., Yang, Y., Wheelan, S.J., Murphy, E., and Steenbergen, C. (2012). Nuclear miRNA regulates the mitochondrial genome in the heart. Circ. Res. *110*, 1596–1603.
8. Gustafsson, A.B., and Gottlieb, R.A. (2008). Heart mitochondria: gates of life and death. Cardiovasc. Res. *77*, 334–343.
9. Grimm, S., and Brdiczka, D. (2007). The permeability transition pore in cell death. Apoptosis *12*, 841–855.
10. Song, R., Hu, X.Q., and Zhang, L. (2019). Mitochondrial MiRNA in Cardiovascular Function and Disease. Cells *8*, 1475.
11. Taganov, K.D., Boldin, M.P., Chang, K.J., and Baltimore, D. (2006). NF-kappaB-dependent induction of microRNA miR-146, an inhibitor targeted to signaling proteins of innate immune responses. Proc. Natl. Acad. Sci. USA *103*, 12481–12486.
12. Pan, J.A., Tang, Y., Yu, J.Y., Zhang, H., Zhang, J.F., Wang, C.Q., and Gu, J. (2019). miR-146a attenuates apoptosis and modulates autophagy by targeting TAF9b/P53 pathway in doxorubicin-induced cardiotoxicity. Cell Death Dis. *10*, 668.
13. Feng, B., Chen, S., Gordon, A.D., and Chakrabarti, S. (2017). miR-146a mediates inflammatory changes and fibrosis in the heart in diabetes. J. Mol. Cell. Cardiol. *105*, 70–76.
14. Li, K., Ching, D., Luk, F.S., and Raffai, R.L. (2015). Apolipoprotein E enhances microRNA-146a in monocytes and macrophages to suppress nuclear factor-κB-driven inflammation and atherosclerosis. Circ. Res. *117*, e1–e11.
15. Hullinger, T.G., Montgomery, R.L., Seto, A.G., Dickinson, B.A., Semus, H.M., Lynch, J.M., Dalby, C.M., Robinson, K., Stack, C., Latimer, P.A., et al. (2012). Inhibition of miR-15 protects against cardiac ischemic injury. Circ. Res. *110*, 71–81.
16. Nishi, H., Ono, K., Iwanaga, Y., Horie, T., Nagao, K., Takemura, G., Kinoshita, M., Kuwabara, Y., Mori, R.T., Hasegawa, K., et al. (2010). MicroRNA-15b modulates cellular ATP levels and degenerates mitochondria via Arl2 in neonatal rat cardiac myocytes. J. Biol. Chem. *285*, 4920–4930.

17. Wang, J.X., Jiao, J.Q., Li, Q., Long, B., Wang, K., Liu, J.P., Li, Y.R., and Li, P.F. (2011). miR-499 regulates mitochondrial dynamics by targeting calcineurin and dynamin-related protein-1. Nat. Med. *17*, 71–78.

18. Lv, G., Shao, S., Dong, H., Bian, X., Yang, X., and Dong, S. (2014). MicroRNA-214 protects cardiac myocytes against H2O2-induced injury. J. Cell. Biochem. *115*, 93–101.

19. Çakmak, H.A., and Demir, M. (2020). MicroRNA and Cardiovascular Diseases. Balkan Med. J. *37*, 60–71.

20. Wang, X., Song, C., Zhou, X., Han, X., Li, J., Wang, Z., Shang, H., Liu, Y., and Cao, H. (2017). Mitochondria Associated MicroRNA Expression Profiling of Heart Failure. BioMed Res. Int. *2017*, 4042509.

21. Wang, X., Ha, T., Liu, L., Zou, J., Zhang, X., Kalbfleisch, J., Gao, X., Williams, D., and Li, C. (2013). Increased expression of microRNA-146a decreases myocardial ischaemia/reperfusion injury. Cardiovasc. Res. *97*, 432–442.

22. Lin, S., and Gregory, R.I. (2015). MicroRNA biogenesis pathways in cancer. Nat. Rev. Cancer *15*, 321–333.

23. Magalhães, P.J., Andreu, A.L., and Schon, E.A. (1998). Evidence for the presence of 5S rRNA in mammalian mitochondria. Mol. Biol. Cell *9*, 2375–2382.

24. Sharma, P., Bharat, Dogra, N. and Singh, S. (2019) Small Regulatory Molecules Acting Big in Cancer: Potential Role of Mito-miRs in Cancer. Curr. Mol. Med. 19, 621–631.

25. Ortega, M.A., Fraile-Martínez, O., Guijarro, L.G., Casanova, C., Coca, S., Álvarez-Mon, M., Buján, J., García-Honduvilla, N., and Asúnsolo, Á. (2020). The Regulatory Role of Mitochondrial MicroRNAs (MitomiRs) in Breast Cancer: Translational Implications Present and Future. Cancers (Basel) *12*, 2443.

26. Zhang, T., Zhang, Y., Cui, M., Jin, L., Wang, Y., Lv, F., Liu, Y., Zheng, W., Shang, H., Zhang, J., et al. (2016). CaMKII is a RIP3 substrate mediating ischemia- and oxidative stress-induced myocardial necroptosis. Nat. Med. *22*, 175–182.

27. Hammarsten, O., Mair, J., Möckel, M., Lindahl, B., and Jaffe, A.S. (2018). Possible mechanisms behind cardiac troponin elevations. Biomarkers *23*, 725–734.

28. Liu, F.Y., Fan, D., Yang, Z., Tang, N., Guo, Z., Ma, S.Q., Ma, Z.G., Wu, H.M., Deng, W., and Tang, Q.Z. (2019). TLR9 is essential for HMGB1-mediated post-myocardial infarction tissue repair through affecting apoptosis, cardiac healing, and angiogenesis. Cell Death Dis. *10*, 480.

29. Peña-Blanco, A., and García-Sáez, A.J. (2018). Bax, Bak and beyond - mitochondrial performance in apoptosis. FEBS J. *285*, 416–431.

30. Meister, G. (2013). Argonaute proteins: functional insights and emerging roles. Nat. Rev. Genet. *14*, 447–459.

31. Srinivasan, H., and Das, S. (2015). Mitochondrial miRNA (MitomiR): a new player in cardiovascular health. Can. J. Physiol. Pharmacol. *93*, 855–861.

32. Bian, Z., Li, L.M., Tang, R., Hou, D.X., Chen, X., Zhang, C.Y., and Zen, K. (2010). Identification of mouse liver mitochondria-associated miRNAs and their potential biological functions. Cell Res. *20*, 1076–1078.

33. Galluzzi, L., Kepp, O., Trojel-Hansen, C., and Kroemer, G. (2012). Mitochondrial control of cellular life, stress, and death. Circ. Res. *111*, 1198–1207.

34. Baines, C.P., Kaiser, R.A., Purcell, N.H., Blair, N.S., Osinska, H., Hambleton, M.A., Brunskill, E.W., Sayen, M.R., Gottlieb, R.A., Dorn, G.W., et al. (2005). Loss of cyclophilin D reveals a critical role for mitochondrial permeability transition in cell death. Nature *434*, 658–662.

35. Schinzel, A.C., Takeuchi, O., Huang, Z., Fisher, J.K., Zhou, Z., Rubens, J., Hetz, C., Danial, N.N., Moskowitz, M.A., and Korsmeyer, S.J. (2005). Cyclophilin D is a component of mitochondrial permeability transition and mediates neuronal cell death after focal cerebral ischemia. Proc. Natl. Acad. Sci. USA *102*, 12005–12010.

36. Devalaraja-Narashimha, K., Diener, A.M., and Padanilam, B.J. (2009). Cyclophilin D gene ablation protects mice from ischemic renal injury. Am. J. Physiol. Renal Physiol. *297*, F749–F759.

OMTN, Volume *23*

Supplemental information

miR-146a inhibits mitochondrial dysfunction and myocardial infarction by targeting cyclophilin D

Qiang Su, Yuli Xu, Ruping Cai, Rixin Dai, Xiheng Yang, Yang Liu, and Binghui Kong

Supplementary Materials

Table S1. Primers used for genotyping

Mouse allele	Primer	Sequence
miR-146a$^{f/f}$	Forward	5′-TACTGTGCGCTCTGTCTCCA-3′
	Reverse	5′-GCAGCCTGAAGTACGTAGCA-3′
Ppif$^{flox/flox}$	Forward	5′-TTCTCACCAGTGCATAGGGCTCTG-3′
	Reverse	5′-GCTTTGTTATCCCAGCTGGCGC-3′
MHC-Cre	Forward	5′-ATGACAGACAGATCCCTCCTATCTCC-3′
	Reverse	5′-CTCATCACTCGTTGCATCATCGAC-3′

Table S2. Primers used for qRT-PCR

Gene	Primer	Sequence
Vdac1	Forward	5′-GCCGCCACATCCTCTGA-3′
	Reverse	5′-AGGCCGTACTCAGTCCATCT-3′
Ant	Forward	5′-AGCGTGAGTTCCATGGTCTG-3′
	Reverse	5′-GACTCCGAAGTAGGCAGCTC-3′
Ppif	Forward	5′-GCGGTATTCAGCTGAGTTGT-3′
	Reverse	5′-GGAGGACTTCGAGGTTGTGT-3′
U6	Forward	5′-ATTGGAACGATACAGAGAAGATT-3′
	Reverse	5′-GGAACGCTTCACGAATTTG-3′
12S rRNA	Forward	5′-AAACTGCTCGCCAGAACACT-3′
	Reverse	5′-TAGGCTGAGCAAGAGGTGGT-3′
Gapdh	Forward	5′-TGTGAACGGATTTGGCCGTA-3′
	Reverse	5′-GATGGTGATGGGTTTCCCGT-3′

Table S3. Microarray analysis of miRNAs induced by ischemic reperfusion in the mitochondria of mice hearts

miRNA	Probe SetID	Signal intensity		Fold change
		Sham	I/R	(I/R vs. Sham)
Upregulated				
miR-150	mmu-miR-150-star_st	428.079	890.627	2.1805
miR-210	mmu-miR-210_st	319.002	1093.851	3.2289
miR-338	mmu-miR-338_st	400.903	960.347	2.2954
miR-92a	mmu-miR-92a-star_st	132.450	399.391	3.1154
miR-696	mmu-miR-669a_st	397.012	972.884	2.5505
miR-532	mmu-miR-532_st	223.051	604.854	2.6117
miR-771	mmu-miR-771-star_st	329.889	689.341	2.2896
miR-450-3p	mmu-miR-450-3p_st	250.858	703.472	2.9042
miR-345-3p	mmu-miR-345-3p_st	141.883	284.888	2.1079
miR-762	mmu-miR-762-star_st	466.012	1024.292	2.2979
Downregulated				
miR-535-5p	mmu-miR-535-3p_st	438.660	182.172	0.4352
miR-330	mmu-miR-330_st	287.856	142.443	0.4748
miR-146a	mmu-miR-146a-star_st	617.733	126.881	0.1953
miR-181a	mmu-miR-181a_st	127.779	58.773	0.4099
miR-34a	mmu-miR-34a-star_st	216.802	74.857	0.3152

I/R, ischemic reperfusion

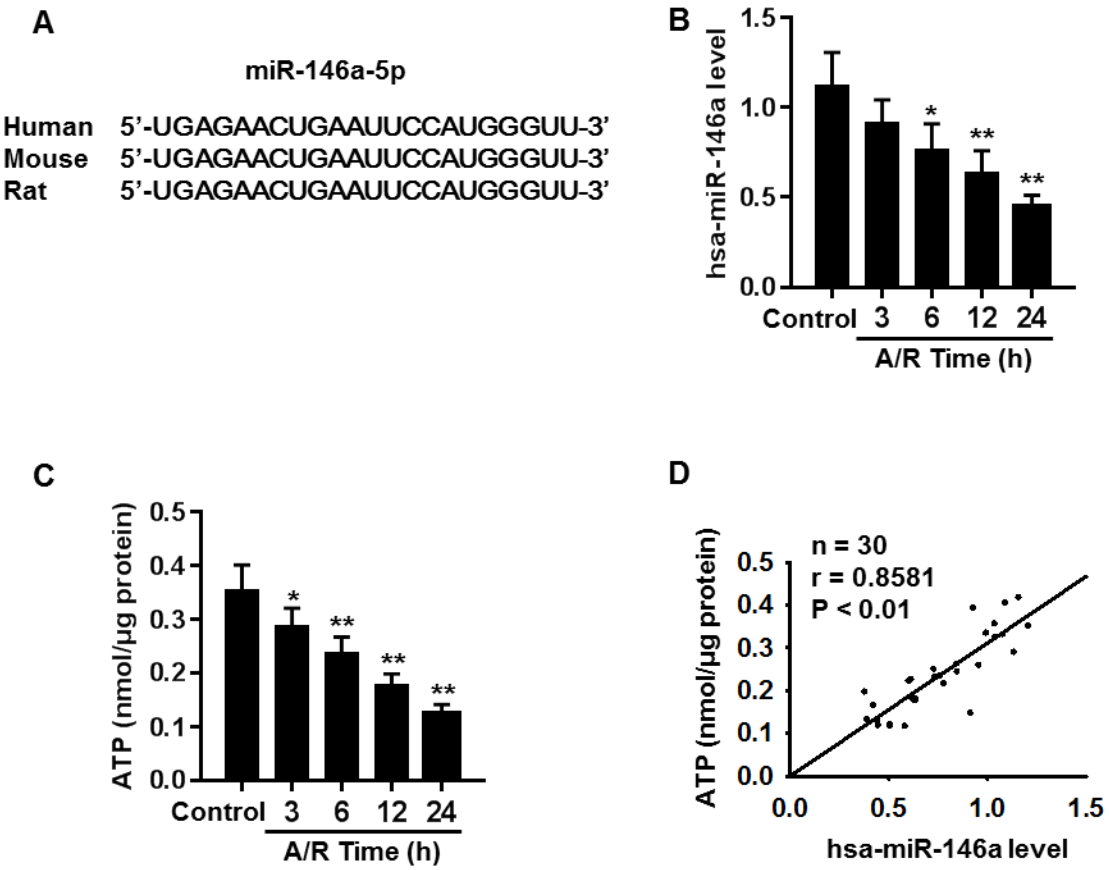

Figure S1 Mitochondrial miR-146a level is associated with mitochondrial dysfunction during cardiac I/R injury. (A) The mature miR-146a-5p strand is conserved between mice and humans. (B and C) Mitochondrial miR-146a level (B) and cellular ATP concentration (C) determined following A/R treatment. Anoxia induced by exposure to 95% N_2 and 5% CO_2 for 24 h, followed by reoxygenation with 95% air and 5% CO_2 for 3, 6, 12 or 24 h. **P* < 0.05, ***P* < 0.01 vs. control, *n* = 6. (D) miR-146a level positively correlates with ATP concentration.

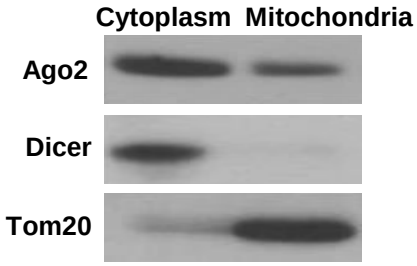

Figure S2 Ago2 and Dicer distribution in mitochondrial and cytosolic fractions. Western blot shows the presence of Ago 2, and absence of Dicer in the mitochondria. Mitochondrial marker protein Tom20 was used as an internal control. *n* = 4.

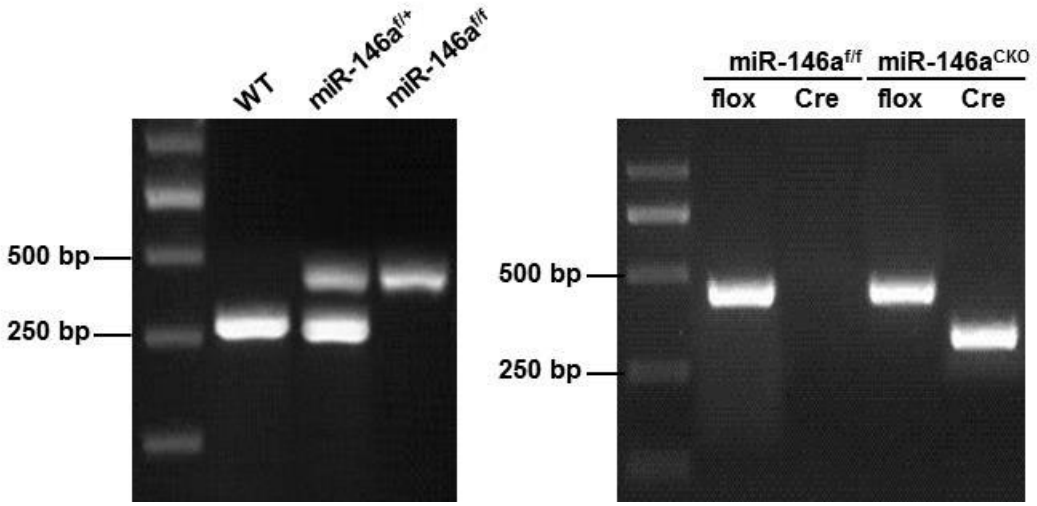

Figure S3 Genotyping analysis of miR-146a cardiomyocyte-specific knockout mice. Examples of DNA band profiles for wild-type (WT), miR-146$^{f/+}$, miR-146a$^{f/f}$, and miR-146a$^{f/f}$/MHC-Cre mice (miR-146a^{CKO}) from PCR analysis of tail biopsies.

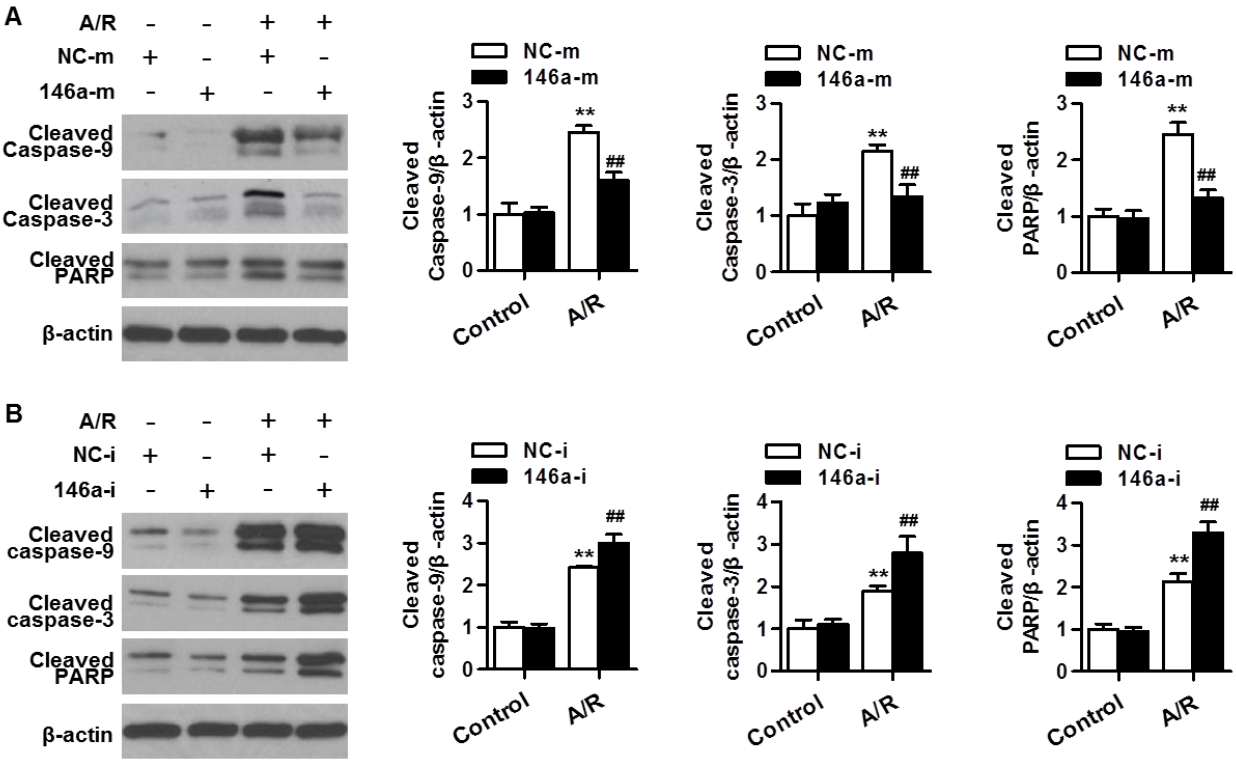

Figure S4 miR-146a regulates activation of caspases induced by A/R stimulation. (A and B) Cardiomyocytes transfected with miR-146a mimic (146a-m, 50 nmol/L, A), miR-146a inhibitor (146a-i, 50 nmol/L, B), or their corresponding negative controls (NC-m or NC-i) 24 h before A/R treatment for 48 h. Western blot analysis of cleaved caspase-9, cleaved caspase-3, and cleaved PARP. $^{**}P < 0.01$ vs. NC-m control or NC-i control; $^{\#\#}P < 0.01$ vs. NC-m A/R or NC-i A/R, $n = 6$.

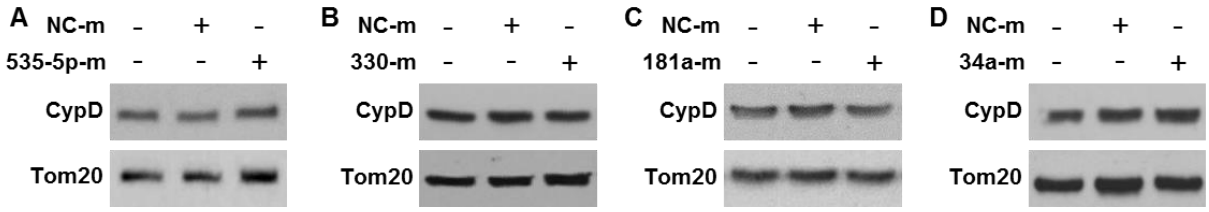

Figure S5 Overexpression of miR-535-5p, miR-330, miR-181a-m or miR-34a does not affect cyclophilin D expression. (A-D) Cardiomyocytes transfected with miR-535-5p mimics, miR-330 mimics, miR-181a mimics, or miR-34a mimics for 48 h. Expression of cyclophilin D was determined by western blot (n = 4).

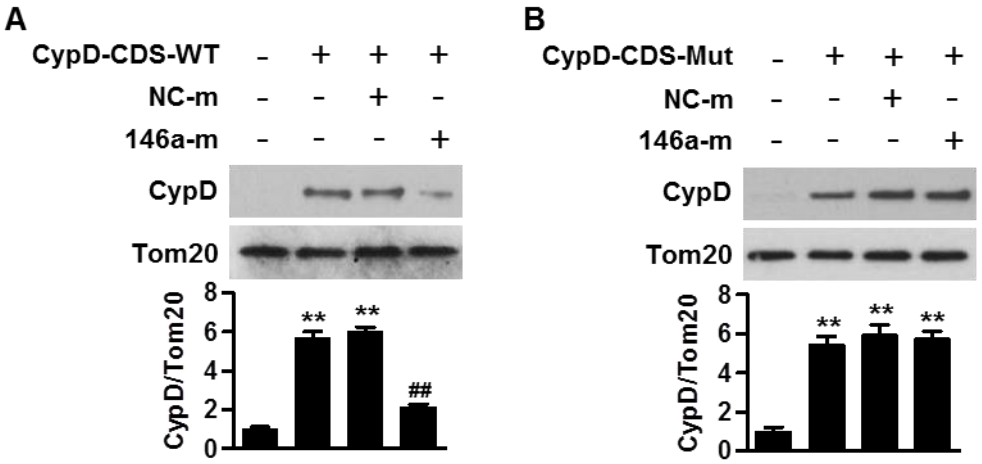

Figure S6 Overexpression of miR-146a does not affect cyclophilin D-CDS-Mut expression. (A and B) Cardiomyocytes co-transfected with the luciferase construct carrying cyclophilin D-CDS-WT (A) or cyclophilin D-CDS-Mut (B) and miR-146a mimic or mimic negative control. Cyclophilin D protein expression analyzed by western blot. $^{**}P < 0.01$ vs. control; $^{\#\#}P < 0.01$ vs. cyclophilin D-CDS-WT, n = 4.

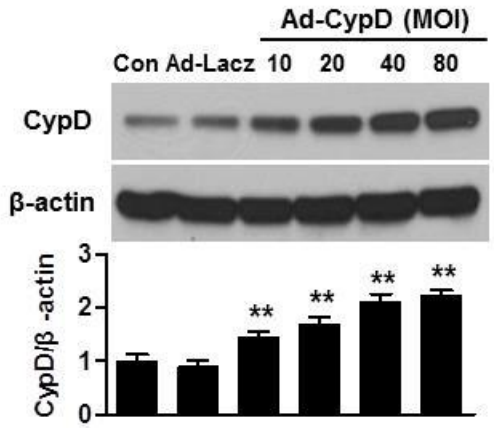

Figure S7 Effect of cyclophilin D adenovirus on cyclophilin D expression in cardiomyocytes. Cardiomyocytes treated with adenoviruses harboring LacZ DNA (Ad-Lacz, at multiplicity of infection [MOI] of 80) or cyclophilin D DNA (Ad-CypD, at MOI of 10, 20, 40, or 80) for 24 h. Cyclophilin D protein expression is shown. ***P* < 0.01 vs. control, $n = 6$.

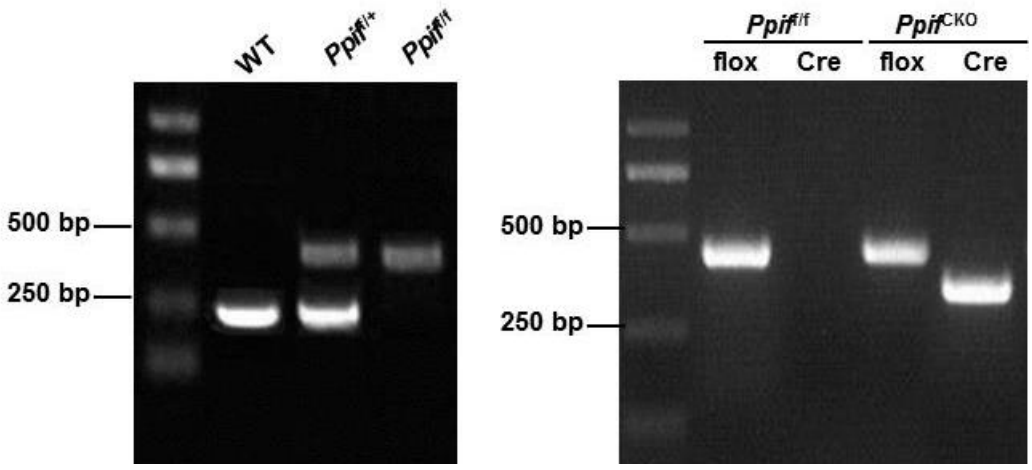

Figure S8 Genotyping analysis of *Ppif* cardiomyocyte-specific knockout mice. Examples of DNA band profiles for wild-type (WT), $Ppif^{f/+}$, $Ppif^{f/f}$, and $Ppif^{f/f}$/MHC-Cre mice ($Ppif^{CKO}$) from PCR analysis of tail biopsies.